

# Precipitation Estimation from the ARM Distributed Radar Network during the MC3E Campaign

SCOTT E. GIANGRANDE

*Atmospheric Sciences Division, Brookhaven National Laboratory, Upton, New York*

SCOTT COLLIS

*Environmental Science Division, Argonne National Laboratory, Argonne, Illinois*

ADAM K. THEISEN

*Atmospheric Radiation Measurement Program Data Quality Office, Cooperative Institute for Mesoscale Meteorological Studies, University of Oklahoma, Norman, Oklahoma*

ALI TOKAY

*University of Maryland, Baltimore County, Baltimore, and NASA Goddard Space Flight Center, Greenbelt, Maryland*

(Manuscript received 23 October 2013, in final form 21 May 2014)

## ABSTRACT

This study presents radar-based precipitation estimates collected during the 2-month U.S. Department of Energy Atmospheric Radiation Measurement Program (ARM)–NASA Midlatitude Continental Convective Clouds Experiment (MC3E). Emphasis is on the usefulness of radar observations from the C-band and X-band scanning ARM precipitation radars (CSAPR and XSAPR, respectively) for rainfall estimation products to distances within 100 km of the Lamont, Oklahoma, ARM facility. The study utilizes a dense collection of collocated ARM, NASA Global Precipitation Measurement, and nearby surface Oklahoma Mesonet gauge records to evaluate radar-based hourly rainfall products and campaign-optimized methods over individual gauges and for areal rainfall characterizations. Rainfall products are also evaluated against the performance of a regional NWS Weather Surveillance Radar-1988 Doppler (WSR-88D) S-band dual-polarization radar product. Results indicate that the CSAPR system may achieve similar point- and areal-gauge bias and root-mean-square (RMS) error performance to a WSR-88D reference for the variety of MC3E deep convective events sampled. The best campaign rainfall performance was achieved when using radar relations capitalizing on estimates of the specific attenuation from the CSAPR system. The XSAPRs demonstrate limited capabilities, having modest success in comparison with the WSR-88D reference for hourly rainfall accumulations that are under 10 mm. All rainfall estimation methods exhibit a reduction by a factor of 1.5–2.5 in RMS errors for areal accumulations over a 15-km<sup>2</sup> NASA dense gauge network, with the smallest errors typically associated with dual-polarization radar methods.

## 1. Introduction

Understanding the properties of clouds and precipitation and simulating their impact on model predictive skill constitute a major challenge for numerical weather prediction, global climate models (GCM), and

cloud-resolving models. The U.S. Department of Energy (DOE) Atmospheric Radiation Measurement Program (ARM) Climate Research Facility outfitted its fixed and mobile global climate facilities with scanning dual-polarized weather radars to better elucidate cloud and precipitation evolution, dynamic and microphysical processes, and longer-term precipitation monitoring (e.g., Ackerman and Stokes 2003; Mather and Voyles 2013). Initial ARM priorities stress the development of a suite of radar hydrological products that include quantitative precipitation estimation (QPE) and associated

---

*Corresponding author address:* Scott Giangrande, Atmospheric Sciences Division, Brookhaven National Laboratory, Bldg. 490D, Bell Ave., Upton, NY 11973.  
E-mail: scott.giangrande@bnl.gov

uncertainty quantification from radar-based QPE methods (e.g., Doviak and Zrníc 1993; Bringi and Chandrasekar 2001). The development of these products is motivated by a demand for high-quality rainfall-accumulation maps to act as a key constraint for continuous climate-model-forcing datasets (e.g., Xie et al. 2004, 2014, manuscript submitted to *J. Geophys. Res.*). There is extensive support for rainfall-accumulation products to evaluate multiple scales of modeling capabilities for the capture of convective cloud life cycle, precipitation regime or diurnal behaviors, and diabatic-heating implications for organized convective systems (Houze et al. 1989; Schumacher et al. 2004; Dai 2006; Milbrandt and Yau 2006; Matsui et al. 2010; Wapler et al. 2010; Bukovsky and Karoly 2011; Dirmeyer et al. 2012; Varble et al. 2011; Iguchi et al. 2012; Del Genio et al. 2012; Caine et al. 2013; Guy et al. 2013).

The recent ARM radar deployment at the Southern Great Plains (SGP) facility near Lamont, Oklahoma, included the placement of a network of three X-band scanning ARM precipitation radars (3-cm wavelength; referred to as XSAPRs herein) and a surveillance C-band scanning ARM precipitation radar (5-cm wavelength; CSAPR herein). This deployment coincided with the joint Midlatitude Continental Convective Clouds Experiment (MC3E), a campaign funded by DOE ARM and the National Aeronautics and Space Administration (NASA) Global Precipitation Measurement (GPM) mission (e.g., Jensen et al. 2010). The field campaign was held from April to June of 2011, with these ARM radars complemented by a suite of GPM ground observations including a dual tipping-bucket rain gauge network that surrounded the SGP site (e.g., Hou et al. 2014). These NASA ground facilities further contributed to a heavily instrumented north-central Oklahoma region that included observations from the Oklahoma Mesonet (e.g., Shafer et al. 2000; Fiebrich et al. 2006) and the operational dual-polarization radars of the National Oceanic and Atmospheric Administration (NOAA) Weather Surveillance Radar-1988 Doppler (WSR-88D) network (S band, 10-cm wavelength, and 70 km west of the ARM facility; e.g., Wilson and Brandes 1979; Whiton et al. 1998; Fulton et al. 1998; Ryzhkov et al. 2005b). The MC3E campaign and existing Oklahoma facilities provided a unique backdrop for evaluating radar-rainfall methods at these radar wavelengths.

A known trade-off for shorter-wavelength radar is that radar rainfall estimation methods necessitate supplementing conventional reflectivity factor  $Z$  estimators with the use of differential phase  $\Phi_{DP}$  (or its product, measurements of specific differential phase  $K_{DP}$ ). These dual-polarization phase measurements are immune to partial attenuation in rain, radar miscalibration, and

partial beam blockages (e.g., Park et al. 2005b; Pepler and May 2012; Vulpiani et al. 2012; Thurai et al. 2012). Previous studies using shorter-wavelength radar have demonstrated the practical advantages of these radars for rainfall estimates within light-to-moderate rain and in the Oklahoma environment (e.g., Matrosov et al. 2006; Wang and Chandrasekar 2010; Borowska et al. 2011). For deep convective precipitation common to Oklahoma, shorter-wavelength radar rainfall estimates may be more susceptible to error as a consequence of hail contamination and significant attenuation in rain. Additional measurement artifacts in deep convection may be associated with nonuniform beamfilling (NBF) and backscatter differential-phase delta contributions to observed differential-phase and reflectivity-factor profiles (Hubbert and Bringi 1995; Ryzhkov and Zrníc 1998; Ryzhkov 2007; Giangrande and Ryzhkov 2008; Wang and Chandrasekar 2009; Otto and Ruschenberg 2011; Giangrande et al. 2013b).

This study builds on the literature for the optimization of rainfall estimation from shorter-wavelength radars. The performance of rainfall estimation techniques from the XSAPRs and the CSAPR is investigated using the MC3E campaign dataset. Traditional QPE uncertainty quantification is performed with comparisons of hourly radar and gauge accumulations. These point characterizations provide a reference for comparing our findings with previous rainfall estimation studies, although the representativeness of gauge-radar comparisons may sometimes be limited (because of systematic or random instrument errors or spatial incompatibilities; e.g., Austin 1987; Anagnostou et al. 1999; Ciach and Krajewski 1999; Krajewski and Smith 2002; Ciach et al. 2007; Seo and Krajewski 2010).

Climate models at resolutions of current and near-future generations of the Intergovernmental Panel on Climate Change modeling capabilities (e.g., Solomon et al. 2007) are coarse when compared with capabilities of surface radar rainfall products. Similar to satellite-platform discussions found in Villarini et al. (2008), it is of interest to test the capabilities of radar rainfall products for the capture of larger-scale mean or areal rainfall properties. This is especially important to spatial scales in better alignment with multigrid weather-resolving models ( $<10\text{--}20\text{ km}^2$ ) that are quickly making a transition into current GCM gridbox ( $>25\text{--}100\text{ km}^2$ ) scales that have similar temporal integration (e.g., hourly or 3 hourly). The dense gauge network available during the MC3E campaign is used to give information on the quality of these areal precipitation measurements. Mean areal rainfall estimates may also be aligned with the strengths of differential-phase-based rainfall estimators. To be specific, improvements in areal products may be

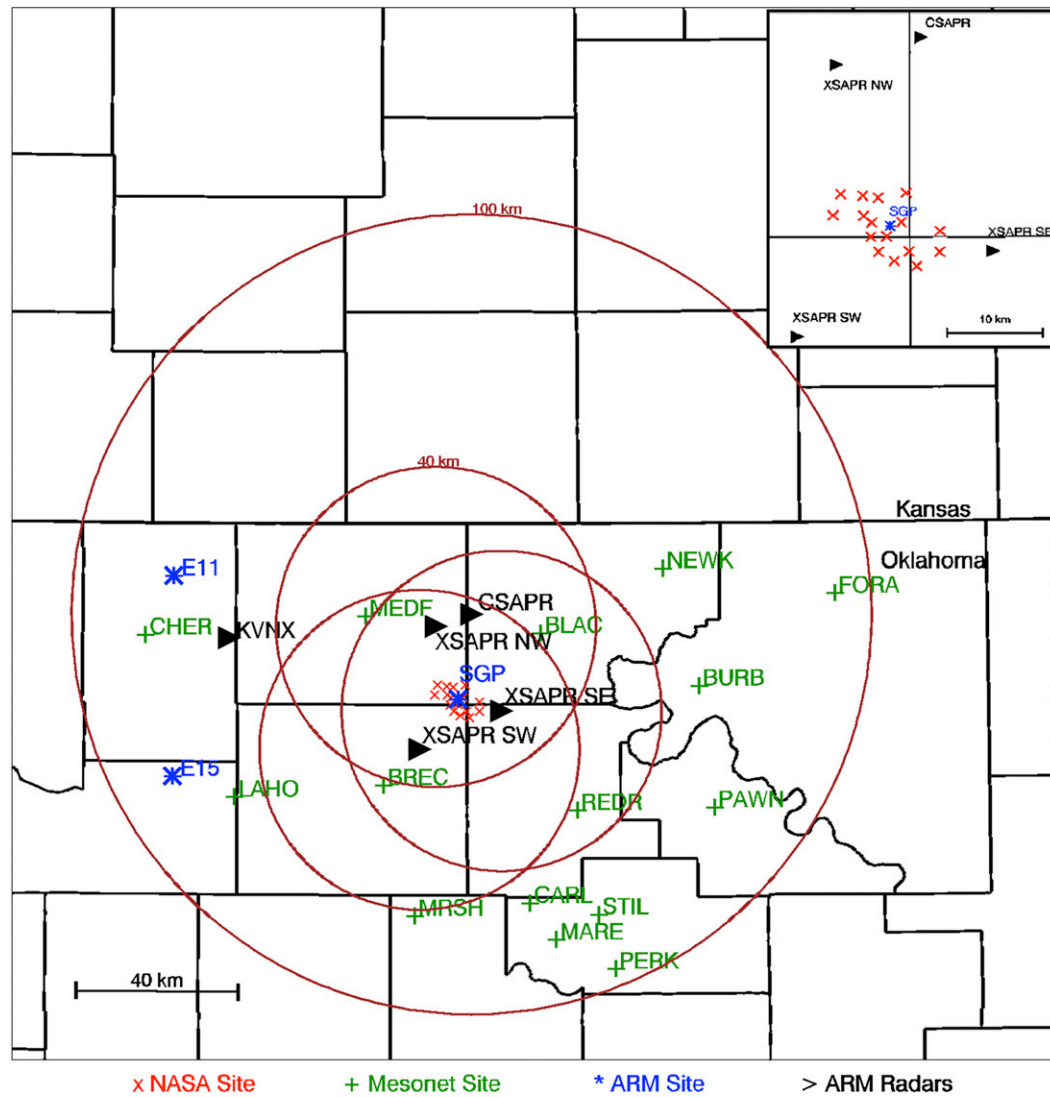


FIG. 1. Schematic of the radar system and gauge locations during the MC3E campaign.

expected since the noisiness in instantaneous or point estimates of specific differential phase can be reduced through spatial or temporal averaging (e.g., Ryzhkov and Zrníc 1998; Giangrande and Ryzhkov 2008; Gourley et al. 2010; Cifelli et al. 2011).

The paper has been organized as follows. The radars, surface instrumentation, and dataset-processing methods are provided in section 2. Section 3 lists the set of rainfall estimation methods matched to the Oklahoma environment that will be evaluated by this study during the MC3E campaign window. Section 4 presents the results of rainfall methods according to traditional point–area rainfall gauge references as well as according to a function of areal-averaging integrations. Discussion and a summary of key findings follow in sections 5 and 6.

## 2. MC3E rainfall dataset and processing

### a. The ARM radars: Dataset and processing

The network of CSAPR and XSAPR radars was located in close proximity to the existing ARM SGP Central Facility (CF) near Lamont (Fig. 1). During the MC3E campaign, 15 precipitation events were sampled (Table 1). The record included the datasets from two XSAPRs [southwest (SW) and southeast (SE)]; the limited coverage of each radar allowed observations of rain during only eight of the campaign events, however. A surveillance CSAPR system was typically functioning simultaneously during this campaign and observed 12 of the events. In total, the MC3E dataset included approximately 40 h (~20 h per radar) of rain coverage from the XSAPRs and 77 h from the CSAPR.

TABLE 1. Listing of MC3E events, highlighting the number of hours recording usable precipitation as captured by the CSAPR and XSAPR SE. Hours in parentheses reflect the available hours over the NASA GPM dense gauge network.

Event date	Precipitation type	KVNX	CSAPR	XSAPR SE
21 Apr 2011	Isolated convective cells	4 (0)	1 (0)	0 (0)
23 Apr 2011	Isolated convective cells	2 (0)	2 (0)	0 (0)
24 Apr 2011	Weak convection, widespread stratiform	15 (7)	15 (7)	2 (1)
25 Apr 2011	Elevated convective cells	14 (13)	12 (13)	3 (2)
26 Apr 2011	Isolated convective cells	3 (2)	3 (2)	2 (2)
27 Apr 2011	Widespread stratiform	10 (8)	10 (8)	2 (1)
1 May 2011	Widespread stratiform	10 (5)	9 (5)	0 (0)
10 May 2011	Weak convection, stratiform	2 (0)	0 (0)	1(0)
11 May 2011	Squall line, stratiform	8 (6)	0 (0)	3 (2)
18 May 2011	Weak convective line	6 (2)	0 (0)	2 (2)
20 May 2011	Squall line, trailing stratiform	15 (9)	10 (6)	5 (4)
23 May 2011	Strong isolated convection	4 (2)	2 (1)	0 (0)
24 May 2011	Strong isolated convection	10 (6)	8 (6)	0 (0)
25 May 2011	Isolated convective cells	5 (3)	3 (3)	0 (0)
31 May 2011	Weak convective line	3 (0)	2 (0)	0 (0)
Total		111 (63)	77 (51)	21 (14)

XSAPR and CSAPR platform specifications include an azimuthal resolution of  $1^\circ$  and range resolution of approximately 100 m. The radar  $Z$  fields were corrected for attenuation in rain by adapting an iterative “hot spot” method as outlined in Gu et al. (2011) that uses processed profiles of  $\Phi_{DP}$  (e.g., Giangrande et al. 2013b). Radar-system  $Z$  miscalibration offsets were believed to be stable and to within 1–2 dBz during MC3E. For this study,  $Z$  corrections were performed by taking advantage of cross-calibration procedures between surface disdrometers and the nearby WSR-88D Vance (Enid, Oklahoma) Air Force Base (AFB) (KVNX) reference (e.g., Ryzhkov et al. 2005a; Giangrande and Ryzhkov 2005). Additional quality checks were performed by consulting the data collected with ARM and NASA GPM profiling radars located at the SGP CF during widespread stratiform periods (e.g., Williams 2012; Giangrande et al. 2013a). All gauge locations were at a sufficient distance from the radars and in regions having no evidence of near-radar ground-clutter contamination for the low grazing angle ( $0.5^\circ$  tilt). For warm-season Oklahoma MC3E events, rainfall observations to within 100 km of the radars at the  $0.5^\circ$  elevation angle displayed no evidence of significant melting-layer contamination. Reflectivity  $Z$  was capped at 53 dBz to mitigate hail contamination (e.g., Giangrande and Ryzhkov 2008).

In addition to typical radar-measurement processing, a calculation for the specific attenuation  $A_H$  was performed along each radial. Rainfall relations that capitalize on specific attenuation are assumed to be less sensitive to variability in drop size distribution than conventional relations. The method that was adopted in this study capitalized on radials of attenuated  $Z$  and filtered  $\Phi_{DP}$  following the formulation described in

Ryzhkov et al. (2014). This method was simple to apply and avoided many known vulnerabilities of other so-called ZPHI rainfall-rate methods (e.g., Testud et al. 2000; Tabary et al. 2011). For the rainfall applications presented in this study,  $A_H$  fields were computed by assuming fixed “alpha” coefficients of  $\alpha = 0.06$  and  $\alpha = 0.2$  at the C-band and X-band wavelengths, respectively (e.g., Park et al. 2005a; Gourley et al. 2007; Ryzhkov et al. 2014). Here, alpha is defined as the ratio of the two-way path-integrated attenuation to the total span of differential phase along the same path. This factor may be interpreted as a bulk value for the ratio of the specific attenuation and specific differential phase  $A_H/K_{DP}$  (e.g., Ryzhkov et al. 2014). This factor alpha (and its optimization) have been used for improved attenuation correction (e.g., Bringi et al. 2001), but this study does not address this role of alpha and its optimization on rainfall estimation performance.

#### b. KVNX WSR-88D dataset

The KVNX Vance AFB WSR-88D underwent an upgrade to dual-polarized capabilities in the months leading up to the MC3E campaign. The KVNX dataset used in this study was the gridded level-III products from that radar that included dual-polarization radar rainfall estimation fields. The record had no temporal gaps during the MC3E campaign or blockages in the direction of the SGP facility (15 events as in Table 1; 101 h of precipitation). This study focuses on the instantaneous precipitation-rate “DPR” product that used the dual-polarization QPE algorithm having a grid resolution of  $0.5 \text{ km}^2$ . Processing for these operational DPR products follows the method of Ryzhkov et al. (2005b). No additional event-based product calibration

or adjustment was performed to modify these products. One known change to the operational code from the Ryzhkov et al. (2005b) study was that the original Oklahoma-tuned rainfall-rate  $R(Z, Z_{DR})$  relationship (applied under light-to-moderate rain conditions:  $Z < 40$  dBz) was replaced with a “tropical”  $R(Z, Z_{DR})$  relationship (e.g., Bringi and Chandrasekar 2001, section 8.1.1). Although this relation is labeled as tropical, the relation has demonstrated solid performance as part of blended relationships in Oklahoma studies during events in which hail contamination on  $Z_{DR}$  measurements was not a factor (e.g., Gourley et al. 2010).

The decision to use the operational rainfall product rather than reprocessing KVNx datasets was motivated by the fact that level-III products were readily accessible and are familiar to the wider weather and climate community. Because the accuracy of operational dual-polarization radar products was relatively unproven in the literature, there was additional benefit to testing these products separate from research-level counterparts (e.g., Cunha et al. 2013). We note that the KVNx differential-phase-processing methods were not as rigorously inspected as those implemented on the ARM datasets. These differences in differential-phase processing may take the form of noisy and/or possibly unphysical WSR-88D-based  $K_{DP}$  estimates. In these situations, the use of  $K_{DP}$  could contribute to the occasional negative rainfall-rate estimate and/or a subsequent lower-quality accumulation. At short temporal or spatial accumulation windows, these known processing issues and associated outlier accumulations imply larger root-mean-square (RMS) errors. For this study, our emphasis was not to improve WSR-88D methods but only to illustrate the quality of shorter-wavelength rainfall products against an operational reference.

### c. MC3E gauge and disdrometer networks: Locations and processing

The MC3E dataset provides a wealth of surface rain gauge and disdrometer references as maintained by several agencies. Figure 1 shows an overview map of the Oklahoma MC3E domain. All MC3E gauge locations that are within a 100-km distance from the SGP CF are shown. The figure inset highlights the dense NASA gauge network deployed in the area surrounding the SGP CF during the MC3E campaign. In total, there were 15 Oklahoma Mesonet gauges located within 100 km of the SGP CF facilities, 3 DOE ARM gauges, and 16 NASA GPM dual rain gauge sites. Additional details on NASA gauge operations can be found in Tokay et al. (2010). Gauge datasets were aggregated from 1- or 5-min rainfall records into hourly accumulations that match to radar rainfall estimation products.

There are multiple sources of errors for tipping-bucket gauge measurements (e.g., Zawadzki 1973; Wilson and Brandes 1979; Austin 1987; Ciach 2003; Sieck et al. 2007), including errors found with gauges operated by the Oklahoma Mesonet, ARM, and NASA GPM during MC3E. In deep convective conditions, errors in gauge accumulations associated with undercatchment due to high winds and splashing may exceed 10% (e.g., Duchon and Essenberg 2001; Duchon et al. 2014). In this study, data quality of the Oklahoma Mesonet, NASA GPM, and DOE ARM gauges is assured through continuous monitoring at those agencies. At hourly scales or longer, it is assumed that tipping-bucket gauge time-sampling errors are not as significant (e.g., Ciach et al. 2007).

### d. Rainfall algorithm performance criteria

To evaluate the conventional and dual-polarization radar rainfall algorithms, we computed several statistics including fractional and absolute differences between radar and gauge estimates (expressed in millimeters; gauge rainfall is considered as reference). Point rainfall estimates were characterized by the bias  $B = \langle \Delta \rangle$  and the RMS error (RMSE)  $= (\langle |\Delta|^2 \rangle)^{1/2}$ . Here,  $\Delta = TR - TG$  is the difference between radar and gauge hourly totals for any given radar–gauge pair, and the angle brackets imply averaging over all such pairs. In a similar way, a fractional bias (FB) and fractional RMS error (FRMSE) were computed by dividing these quantities by the mean gauge accumulation  $\langle TG \rangle$ . An absolute bias was computed as  $|B| = \langle |\Delta| \rangle$ . A standard calculation of a Pearson correlation coefficient  $r$  was also performed. For the purpose of this study, a radar “point” measurement was defined by averaging the two radials and five range gates (10 gates in total) that are nearest to each gauge measurement (typically 0.5–1 km<sup>2</sup>). An accumulation threshold of 1 mm was placed on the gauge accumulations such that hours recording below this threshold were removed from our point–gauge analyses. This threshold ensured that at least four tips were recorded for each gauge observation within the hour. For KVNx products, the rainfall estimate from the closest grid box was the one selected. The performance for point metrics was also segregated according to rainfall accumulation totals in a way similar to that of Ryzhkov et al. (2005b) to better explore bias and errors from light-to-heavier rain conditions.

Error estimate comparisons were also performed for “areal” rainfall behaviors. Determining an appropriate number of surface gauges to establish a “true” areal-average rainfall behavior has been previously discussed in studies such as Zawadzki (1973), Rodríguez-Iturbe and Mejía (1974), and Villarini et al. (2008). During the MC3E campaign, the GPM ground network was

distributed over an approximately 15-km<sup>2</sup> grid at close distance to the radars. As in the estimates of Villarini et al. (2008), this number of gauges for an hourly accumulation in moderate precipitation may provide a good representation of true rainfall behavior to within 20% accuracy. Our emphasis was on hourly areal averages calculated by taking the mean of the hourly GPM gauge accumulations and then comparing these with the averaged hourly radar estimates. Each valid hour required a minimum of one gauge to have recorded four or more tips. Additional evaluations of the performance of KVN<sub>X</sub> areal rainfall estimates for 1- and 3-h temporal aggregations were considered over the GPM gauge network.

### 3. Rainfall algorithms

The conventional and dual-polarized radar rainfall relations evaluated in this study are listed in Table 2. The  $R(Z)$  and  $R(K_{DP})$  relations were compiled from previous studies conducted in Oklahoma warm-season and deep-convective rainfall at C band (e.g., Gu et al. 2011) and X band (e.g., Park et al. 2005a,b; Wang and Chandrasekar 2010). These relations include formulations for rainfall estimates as a function of specific attenuation  $A_H$  as proposed by Ryzhkov et al. (2014) for temperature  $T = 20^\circ\text{C}$  and fixed alpha coefficients as in the previous section. Relationship forms that capitalize on CSAPR or XSAPR  $Z_{DR}$  measurements are avoided in this study. This is a consequence of poor measurement quality associated with significant differential attenuation in rain and inadequate  $Z_{DR}$  correction procedures for MC3E events. Standard relation forms as in Table 2 are as follows:

$$R(Z) = aZ^b, \tag{1}$$

$$R(K_{DP}) = cK_{DP}^d, \text{ and} \tag{2}$$

$$R(A_H) = eA_H^f, \tag{3}$$

where  $Z$  in Eq. (1) is in linear units ( $\text{mm}^6 \text{m}^{-3}$ ),  $K_{DP}$  is in degrees per kilometer,  $A_H$  is in decibels per kilometer, and coefficients  $a$ – $f$  are replaced by associated values in Table 2 for CSAPR and XSAPRs, respectively.

In addition to single-variable dual-polarization relations, “synthetic” (also termed “hybrid” or “blended”) relationships for Oklahoma were tested (e.g., Ryzhkov et al. 2005b). The idea of using the strengths of multiple relations to optimize rainfall estimation [as suggested by Chandrasekar et al. (1993), Cifelli et al. (2002), Matrosov et al. (2005), Park et al. (2005b), and others] was further explored by Ryzhkov et al. (2005b,c) for Oklahoma. Note that the KVN<sub>X</sub> radar rainfall product adopts this synthetic

TABLE 2. Coefficients for selected rainfall algorithms employed for this study.

Algorithm	CSAPR	XSAPR
$R(Z)$	$0.017Z^{0.714}$	$0.029Z^{0.67}$
$R(K_{DP})$	$25.1K_{DP}^{0.777}$	$16.9K_{DP}^{0.801}$
$R(A_H)$	$294.0A_H^{0.89}$	$43.5A_H^{0.79}$

approach to rainfall estimation. According to this synthetic algorithm approach, the choice between various optimized dual-polarization rainfall relations was determined by a radar reflectivity  $Z$  threshold used as a proxy for storm intensity/regime. For S-band studies, Ryzhkov et al. (2005b) recommend using  $R(Z, Z_{DR})$  relations in light-to-moderate rain [e.g.,  $Z < 40 \text{ dBz}$ ;  $R(Z) < 12 \text{ mm h}^{-1}$ ] and  $R(K_{DP})$ -based relations in heavier rainfall (e.g.,  $Z > 40 \text{ dBz}$ ). At shorter wavelengths, the construction has been simpler, placing less emphasis on  $Z$  fields as

$$R(Z), Z \leq 30 \text{ dBz}, \text{ and}$$

$$R(K_{DP}), Z > 30 \text{ dBz}, \tag{4}$$

where Eq. (4) is used on CSAPR datasets (e.g., Park et al. 2005a,b). For XSAPR datasets,  $R(Z)$  was used up to  $Z \leq 35 \text{ dBz}$  to better match the Park et al. (2005b) study.

### 4. Performance of radar rainfall estimates

#### a. Point-gauge comparisons

Point comparison scatterplots for the campaign events in Table 1 are provided in Figs. 2–5. The corresponding rainfall statistics are found in Table 3. Figure 2 shows the CSAPR performance as compared with the Oklahoma Mesonet gauge network, GPM tipping-bucket rain gauge sites, and gauge sites for 1) the conventional  $R(Z)$  method in Eq. (1), 2) a  $K_{DP}$ -based method in Eq. (2), 3) the Ryzhkov et al. (2014)-type specific-attenuation-based method in Eq. (3), and 4) a basic synthetic-type rainfall method as in Eq. (4). Figures 3 and 4 provide the corresponding rainfall estimation performances for the two XSAPRs.

The performance of the KVN<sub>X</sub> rainfall product with respect to campaign gauges is found in Figs. 5a and 5b. Figure 5a shows this KVN<sub>X</sub> performance over the 823 gauge comparison points matched to the hours and gauges observed by the CSAPR system. For Fig. 5b, the KVN<sub>X</sub> performance is matched to the hours and gauges as captured by the XSAPR SE (228 hourly point comparisons). The XSAPR SE and XSAPR SW results were found to be nearly identical when compared with the available MC3E KVN<sub>X</sub> reference. The remainder of

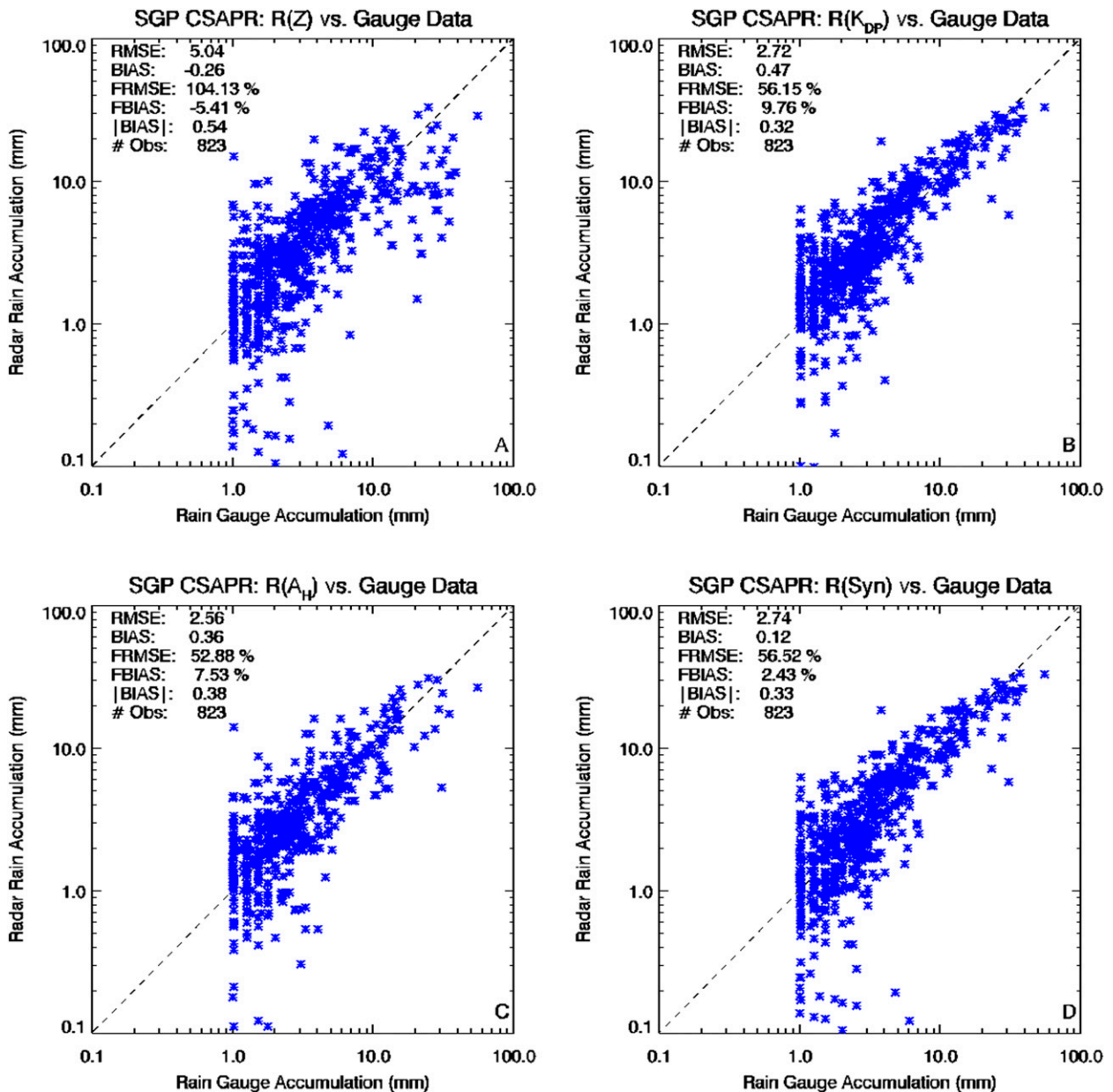


FIG. 2. Scatterplot of point-estimate hourly radar–gauge results observed by the CSAPR over the available gauge network during the MC3E period for an (a)  $R(Z)$ , (b)  $R(K_{DP})$ , (c)  $R(A_H)$ , and (d)  $R(\text{synthetic})$  method.

this study will highlight the results from the XSAPR SE dataset, which offered additional hours of gauge sampling.

In addition to cumulative scatterplot and tabular performances, Table 4 segregates the performance of the rainfall algorithms according to the gauge accumulation. Here, we partition rainfall into four intervals of hourly accumulation having  $1 < R < 5$  mm,  $5 < R < 10$  mm,  $10 < R < 20$  mm, and  $R > 20$  mm. Results are provided for KVN<sub>X</sub> according to the matching radar–gauge paired samples, respectively.

#### b. Areal–gauge comparisons

Figures 5c, 5d, 6, and 7 show the areal rainfall performance over the dense network of NASA GPM gauges for the KVN<sub>X</sub>, CSAPR, and the XSAPR SE products, respectively. A summary of areal performance with respect to the tested algorithms is documented in Table 5. Once again, the performance of the XSAPR SW was found to be nearly identical to that of the XSAPR SE despite having a different viewing angle of the precipitation. This result provides additional confidence in the

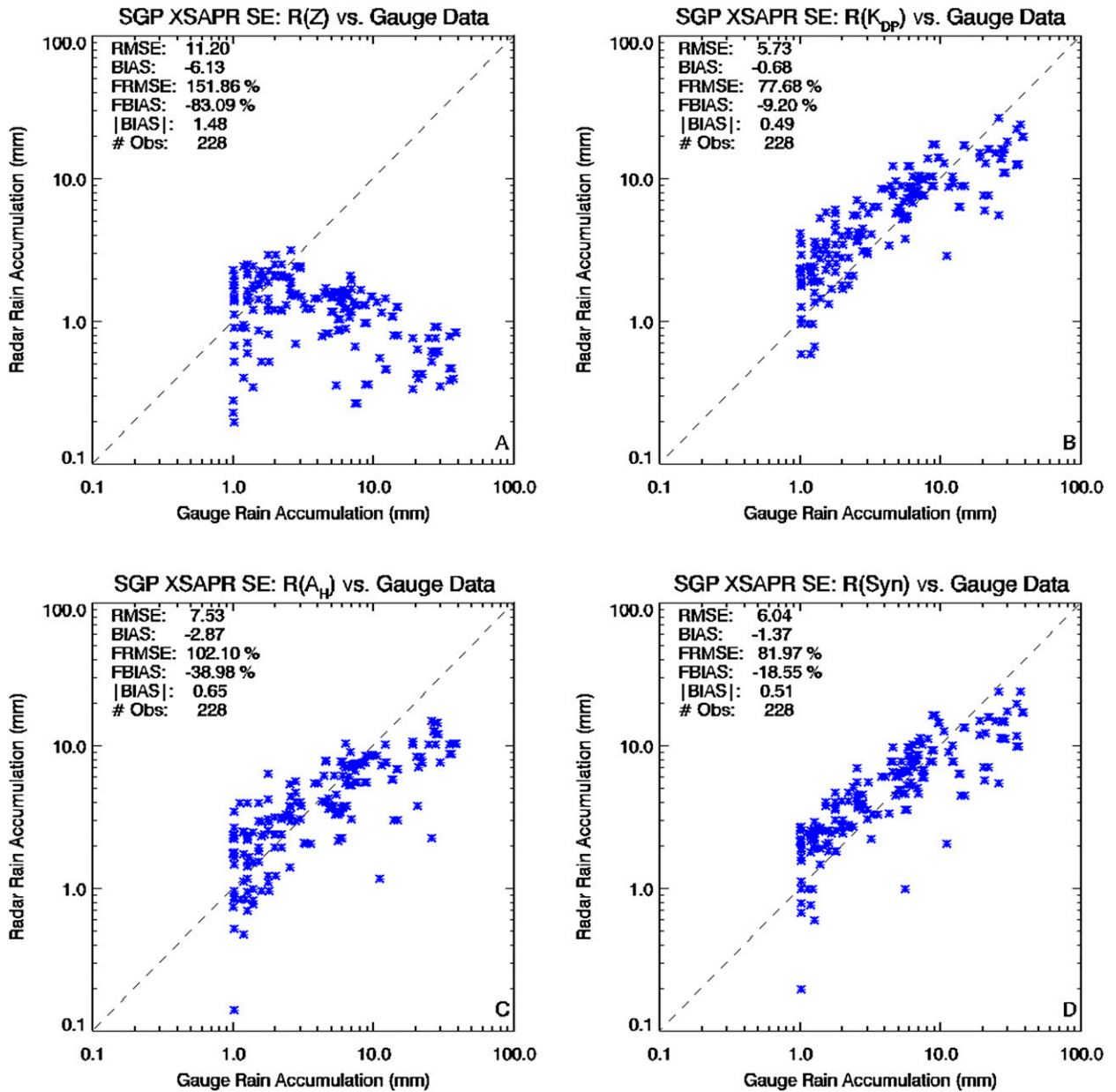


FIG. 3. As in Fig. 2, but for available gauges observed by the XSAPR SE radar.

relative radar error characteristics for these specific campaign events.

In addition to the point and areal hourly accumulation performances, we consider the quality of areal rainfall products collected over 3-h accumulation windows. Because these extended spatial-temporal 3-h areal averages are not feasible for the ARM radars during MC3E (sampling limitations), an additional check for 3-hourly accumulations was performed using only the nearby KVN<sub>X</sub> reference. Figure 8 provides scatterplots for the areal performance of hourly versus regularly spaced 3-h

accumulation windows (63 individual hours having 35 associated 3-hourly windows).

**5. Discussion**

The performance of an unattenuated KVN<sub>X</sub> reference during MC3E was in line with previous expectations for Oklahoma warm-season events (e.g., Ryzhkov et al. 2005b; Giangrande and Ryzhkov 2008; Vulpiani et al. 2009). This campaign reference (e.g., RMSE = 4.14 mm; |B| = 0.5 mm) did not benefit from case-specific

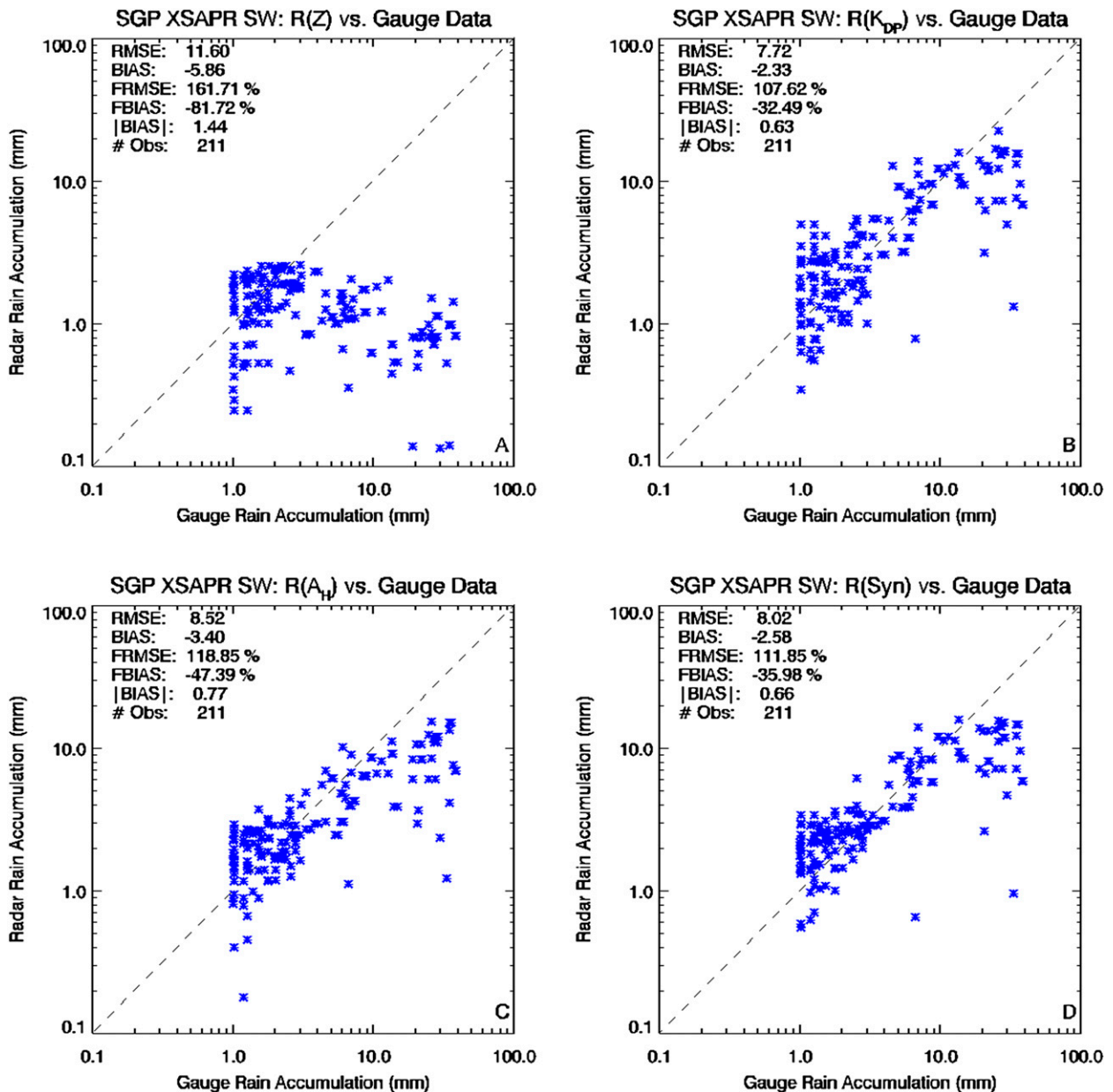


FIG. 4. As in Fig. 3, but for the XSAPR SW radar.

calibration to improve the relative performance in light-to-moderate Oklahoma rainfall (e.g., Table 3). We find a stable absolute bias on the order of 0.5 mm for all accumulation windows (e.g., Table 4). KVN<sub>X</sub> products overestimated rainfall at the lower accumulations and underestimated accumulations at higher relative gauge accumulations, however. These behaviors were consistent with those of the constituent rainfall relations used in the synthetic approach that makes a transition from an  $R(Z, Z_{DR})$ -based method at lower rainfall rates to an  $R(K_{DP})$  relation at higher rainfall rates. For this study,

RMSE performance improved by a factor of 2.5–3 for areal rainfall accumulation averages at the 15-km<sup>2</sup> scale. Limited improvement may be attributed to the spatial averaging that supports reduction of instantaneous noisiness and/or nonuniform beamfilling effects on  $K_{DP}$ -based estimates (e.g., Ryzhkov and Zrnic 1998; Ryzhkov et al. 2005b).

The CSAPR rainfall products outperformed the nearby KVN<sub>X</sub> reference product according to most gauge reference metrics (e.g., Tables 3, 4). This favorable showing may have been influenced by several factors that

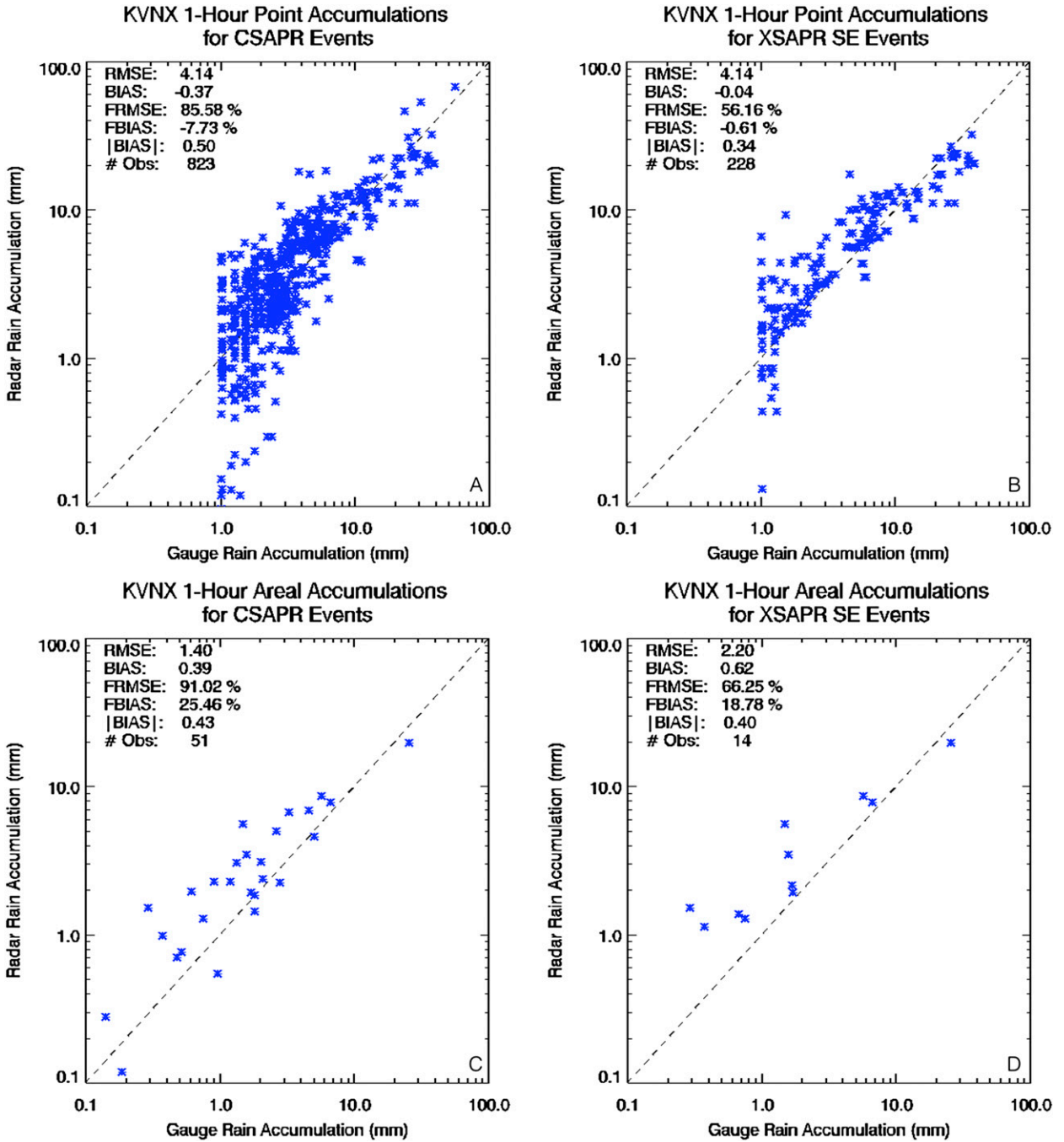


FIG. 5. Matched (top) point–gauge and (bottom) areal–gauge scatterplot results associated with the reference KVNX DPR radar product for (a), (c) CSAPR and (b), (d) XSAPR SE conditions.

include 1) the closer proximity of the CSAPR system to the matching gauge locations, 2) careful radar  $Z$  calibrations performed for each event, and 3) limited sampling of extreme events that have accumulations greater than 20 mm and/or events associated with severe attenuation in rain resulting in signal extinction at C band. CSAPR-based methods demonstrated a substantial

improvement in bias and RMSE at gauge accumulations between 5 and 20 mm.

This study highlights the success of single-parameter Oklahoma-specific relations that are based on estimates of  $K_{DP}$ , as well as those based on the relatively unproven  $A_H$  rainfall retrieval techniques. The CSAPR  $A_H$ -based rainfall estimates are the optimal selection for the MC3E

TABLE 3. Algorithm performance for point-gauge estimates for the KVN, CSAPR, and XSAPR SE. Here, SYN indicates synthetic.

Radar algorithm	Obs	RMSE	Bias	FRMSE	Fbias	B
KVN DPR (CSAPR)	823	4.14	-0.37	85.58	-7.73	0.50
CSAPR $R(Z)$	823	5.04	-0.26	104.13	-5.41	0.54
CSAPR $R(K_{DP})$	823	2.72	0.47	56.15	9.76	0.32
CSAPR $R(A)$	823	2.56	0.36	52.88	7.53	0.38
CSAPR $R(SYN)$	823	2.74	0.12	56.52	2.43	0.33
KVN DPR (XSAPR SE)	228	4.14	-0.04	56.16	-0.61	0.34
XSAPR SE $R(Z)$	228	11.20	-6.13	151.86	-83.09	1.48
XSAPR SE $R(K_{DP})$	228	5.73	-0.68	77.68	-9.20	0.49
XSAPR SE $R(A)$	228	7.53	-2.87	102.10	-38.98	0.65
XSAPR SE $R(SYN)$	228	6.04	-1.37	81.97	-18.55	0.51

datasets, showing superior RMSE (=2.56 mm) and minimal bias (e.g.,  $|B| = 0.38$  mm) performance over a wide range of MC3E rainfall conditions (e.g., Fig. 2; Tables 3, 4). This result is encouraging since these methods require very simple construction and negligible tuning. The result gives further motivation for investigation of Ryzhkov et al. (2014) techniques and efforts to include sensitivity studies for the selection, control, and optimization of alpha coefficients and temperature constraints.

The Oklahoma-matched  $K_{DP}$ -based relationship demonstrated a sizable improvement over the KVN reference (e.g., RMSE = 2.72 mm and  $|B| = 0.32$  mm). For this dataset, the relation was less optimal in light-to-moderate rain (e.g., gauge accumulations < 10 mm; Table 4) but was the preferable choice when considering higher rain accumulations. These higher-accumulation conditions were likely those consistent with the presence of hail or attenuation hot-spot challenges known for  $A_H$  fields. This behavior was not surprising, matching with theoretical rainfall performance discussions as presented in Ryzhkov et al. (2014).

For areal rainfall performance metrics, the CSAPR relations demonstrated less of a relative improvement as compared with KVN (factor of 2–2.5 reduction in RMSE). One simple explanation was that specific differential phase was more reliably estimated from the CSAPR than from typical KVN processing (minimizing the need for noise reduction through spatial-temporal averaging). For this study, the CSAPR synthetic methods did not meaningfully outperform single-parameter relations. The possible benefits of the synthetic approach may have been masked, however, because of the removal of light-rain conditions (problematic for phase-based rainfall estimates) if using a 1-mm gauge accumulation threshold.

A calculation for the linear correlation coefficient between CSAPR radar products and gauge hourly accumulations gives additional confidence for the solid

TABLE 4. As in Table 3, but for relationships as a function of total accumulation.

Radar algorithm	1–5 mm	5–10 mm	10–20 mm	>20 mm	1–5 mm	5–10 mm	10–20 mm	>20 mm
	No. of obs				Absolute bias			
KVN DPR	623	110	51	39	0.59	0.41	0.5	0.42
CSAPR $R(Z)$	623	110	51	39	0.49	0.39	0.4	0.9
CSAPR $R(K_{DP})$	623	110	51	39	0.41	0.32	0.18	0.23
CSAPR $R(A)$	623	110	51	39	0.43	0.26	0.29	0.5
XSAPR SE $R(Z)$	127	55	17	29	0.57	1.36	1.74	1.92
XSAPR SE $R(K_{DP})$	127	55	17	29	0.58	0.27	0.32	0.62
XSAPR SE $R(A)$	127	55	17	29	0.42	0.26	0.62	1.01
	RMSE				FRMSE			
KVN DPR	2.04	3.67	7.59	13.48	86.95	57.14	56.99	46.42
CSAPR $R(Z)$	2.05	3.95	6.1	19.38	87.43	61.45	45.81	66.74
CSAPR $R(K_{DP})$	1.69	2.89	3.23	8.5	72.39	45.01	24.28	29.27
CSAPR $R(A)$	1.54	2.44	4.14	7.79	65.8	37.98	31.06	26.84
XSAPR SE $R(Z)$	1.31	5.6	13.28	28.55	66.61	83.67	95.68	100.2
XSAPR SE $R(K_{DP})$	2.05	2.88	4.57	14.53	104.13	43.08	32.96	51.02
XSAPR SE $R(A)$	1.24	1.95	7.35	19.99	62.86	29.21	52.96	70.17
	Bias				Fbias			
KVN DPR	0.25	0.15	-4.09	-7.09	10.97	2.4	-30.72	-24.43
CSAPR $R(Z)$	0.63	1.41	-1.65	-17.5	27.04	22.06	-12.4	-60.27
CSAPR $R(K_{DP})$	0.67	1.37	0.64	-5.51	28.63	21.44	4.86	-18.98
CSAPR $R(A)$	0.51	0.83	0.12	-10.13	21.8	13.04	0.91	-34.9
XSAPR SE $R(Z)$	-0.53	-5.43	-12.94	-27.91	-27.22	-81.16	-93.24	-97.98
XSAPR SE $R(K_{DP})$	1.44	1.95	-3.06	-13.55	73.1	29.15	-22.04	-47.57
XSAPR SE $R(A)$	0.57	-1.1	-6.61	-19.15	29.2	-16.48	-47.64	-67.2

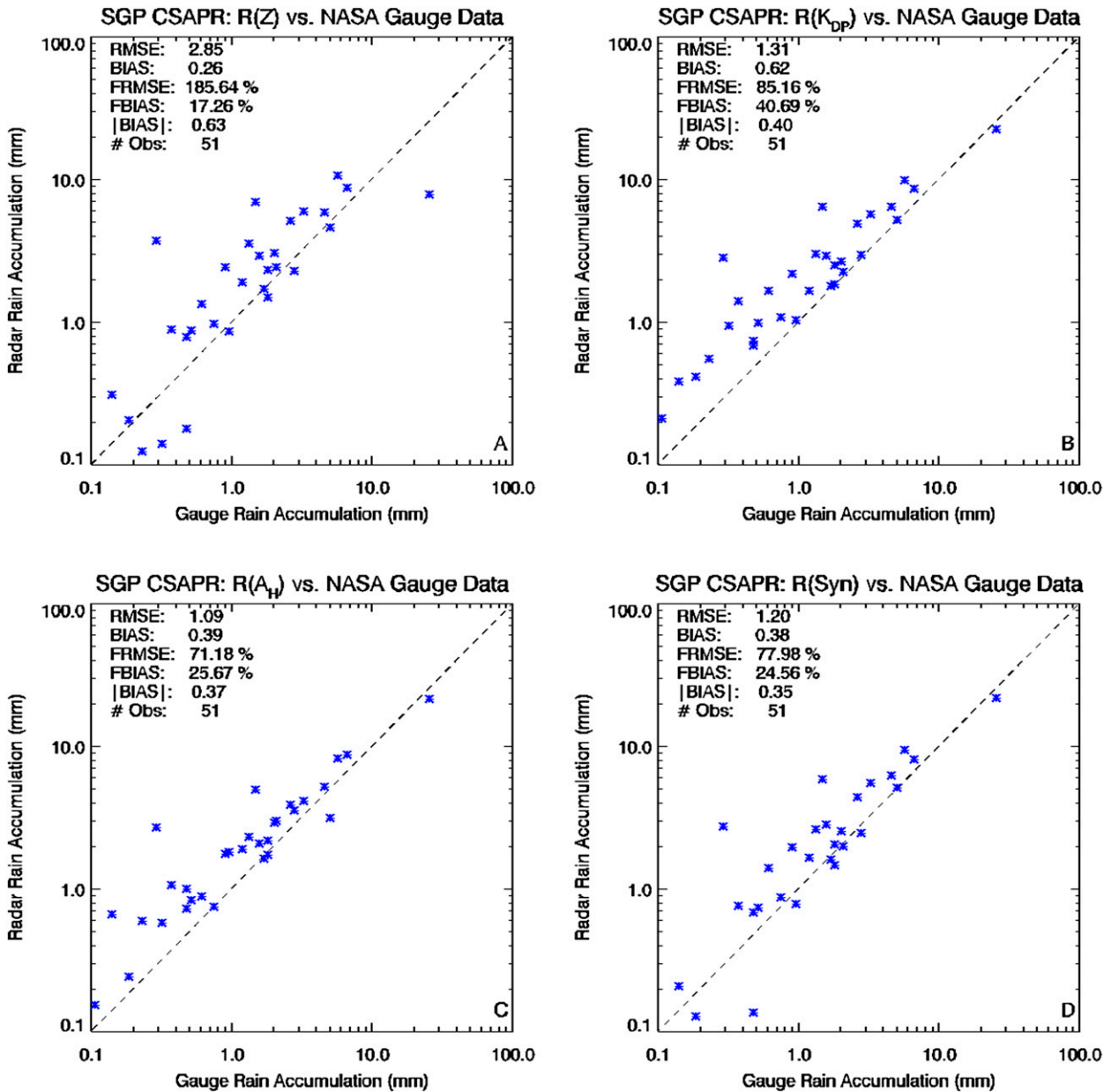


FIG. 6. As in Fig. 2, but for areal performance over available campaign NASA domain hours.

ARM rainfall performance ( $r \approx 0.8\text{--}0.9$ ). These correlation values were slightly larger than those calculated between the KVN<sub>X</sub> product and gauge references ( $r$  of  $\sim 0.79$ ). Cross comparisons between the hourly CSAPR point performances and the corresponding KVN<sub>X</sub> accumulations highlighted a modest radar-to-radar estimate bias. CSAPR consistently estimated higher accumulations as compared with KVN<sub>X</sub>, while having RMSEs of similar magnitude to hourly KVN<sub>X</sub>-to-gauge comparisons. Additional linear correlation-coefficient calculations between the various radar platform-based estimates showed mixed

results. The highest relative correlations ( $r$  of  $\sim 0.74$ ) were found between the KVN<sub>X</sub> product and CSAPR  $R(K_{DP})$  methods. The lowest correlations ( $r$  of  $\sim 0.51$  and  $0.59$ ) were found between the KVN<sub>X</sub> and  $R(A_H)$  and  $R(Z)$  products, respectively. Some uncertainty can be attributed to low accumulations that do not favor KVN<sub>X</sub> or CSAPR products.

XSAPR products were found to be vulnerable to attenuation in rain through deep Oklahoma convective cells. It was common to observe complete beam extinction in the direction of campaign gauges during

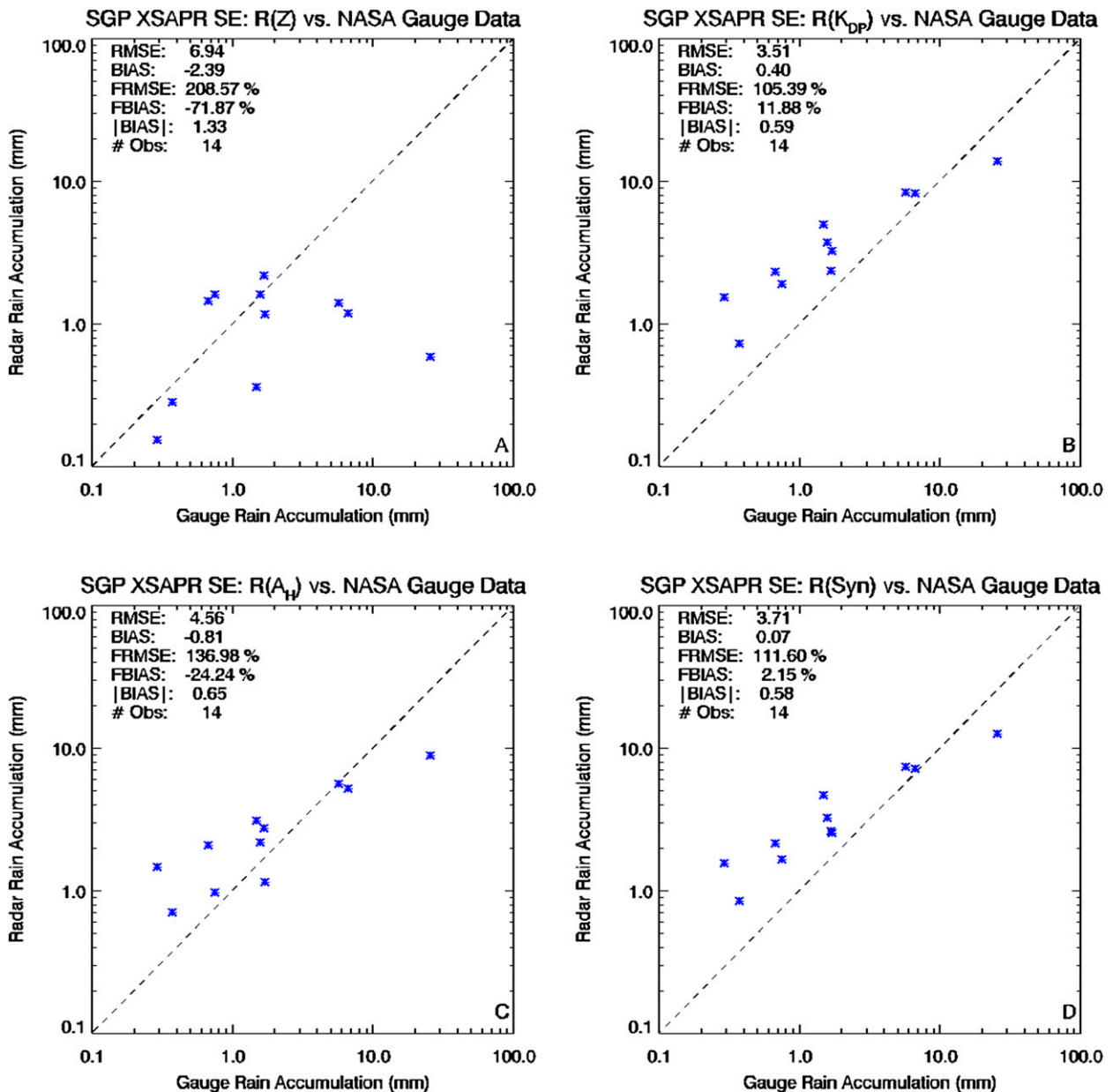


FIG. 7. As in Fig. 3, but for areal performance over available campaign NASA domain hours.

several convective events (as in Fig. 9 for the 20 May 2011 squall line). In response, the corresponding estimators demonstrated systematic negative biases (underestimation) and higher relative RMSE. Although XSAPR rainfall estimation performance improved when capitalizing on dual-polarization variables, these relations demonstrated bias and RMSE that reflected a systematic rainfall underestimation (as compared with KVN<sub>X</sub> and CSAPR performance). Nevertheless, XSAPR performance under light-to-moderate rain conditions (absent significant attenuation in rain) was found to be comparable to KVN<sub>X</sub> and CSAPR references. Areal

XSAPR estimates demonstrated the lowest factors of improvement in RMSE (~1.5). Here, this result was expected since areal XSAPR averaging did not appear to reduce systematic errors associated with pervasive attenuation in rain or complete beam extinction.

The ARM climate community places significant importance on establishing the rainfall-product uncertainty to larger scales. The authors suggest that the errors found for Oklahoma events provide a reasonable example of a worst-case challenge for a remote ARM radar deployment. It is encouraging that radar point and areal behaviors match well to the basic calculations of

TABLE 5. As in Table 3, but for areal performance over NASA gauge network.

Radar algorithm	Obs	RMSE	Bias	FRMSE	Fbias	B
KVNX DPR (CSAPR)	51	1.40	0.39	91.02	25.46	0.43
CSAPR $R(Z)$	51	2.85	0.26	185.64	17.26	0.63
CSAPR $R(K_{DP})$	51	1.31	0.62	85.16	40.69	0.40
CSAPR $R(A)$	51	1.09	0.39	71.18	25.67	0.37
CSAPR $R(SYN)$	51	1.20	0.38	77.98	24.56	0.35
KVNX DPR (XSAPR SE)	14	2.20	0.62	66.25	18.78	0.40
XSAPR SE $R(Z)$	14	6.94	-2.39	208.57	-71.87	1.33
XSAPR SE $R(K_{DP})$	14	3.51	0.40	105.39	11.88	0.59
XSAPR SE $R(A)$	14	4.56	-0.81	136.98	-24.24	0.65
XSAPR SE $R(SYN)$	14	3.71	0.07	111.60	2.15	0.58

uncertainty for an unattenuated KVNX reference under many circumstances (e.g., Table 4). For the future ARM user, this argues that a well-calibrated extended areal rainfall estimation product is likely an unbiased estimate of the rainfall. As a function of the hourly accumulation, our findings suggest an estimate accuracy that is often only within 50% of gauge truth. Again, this performance only considers shorter-wavelength methods in the

presence of significant attenuation in rain and in a challenging Oklahoma environment. Because these MC3E results suggest a similar or improved level of performance relative to that of the current KVNX, it may be the case that this level of performance is close to the best that can be achieved without event-specific tuning of coefficients. Additional testing of possible error reduction over longer temporal accumulation windows is illustrated by the comparison of 1- versus 3-h KVNX performance in Fig. 8. These examples did not reveal a substantial improvement in bias or RMSE when considering extended spatial-temporal averaging, but expectation of a substantial improvement is likely unrealistic when sampling isolated and intense deep-convective storms that quickly transit over similar small-sized domains.

6. Conclusions

Radar QPE product development is motivated by a growing demand for rainfall products as constraints to continuous climate-model-forcing datasets and as a means to evaluate multiple scales of modeling capabilities. As a reference for the potential quality of dual-polarized rainfall products from shorter-wavelength radars, this study explores rainfall products as collected during the DOE ARM and NASA GPM MC3E campaign. This campaign was undertaken in a challenging Oklahoma environment wherein these radars were complemented by

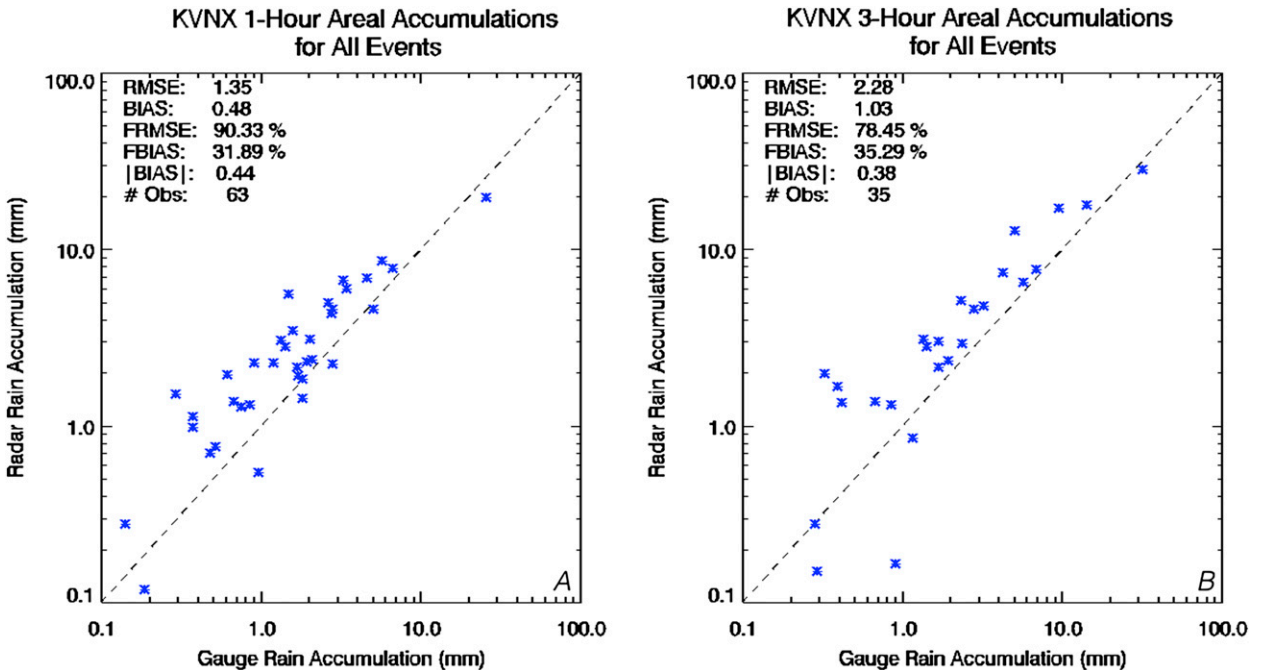


FIG. 8. (a) 1- and (b) 3-h areal comparison over all available MC3E campaign hours as viewed from the KVNX radar over the NASA gauges.

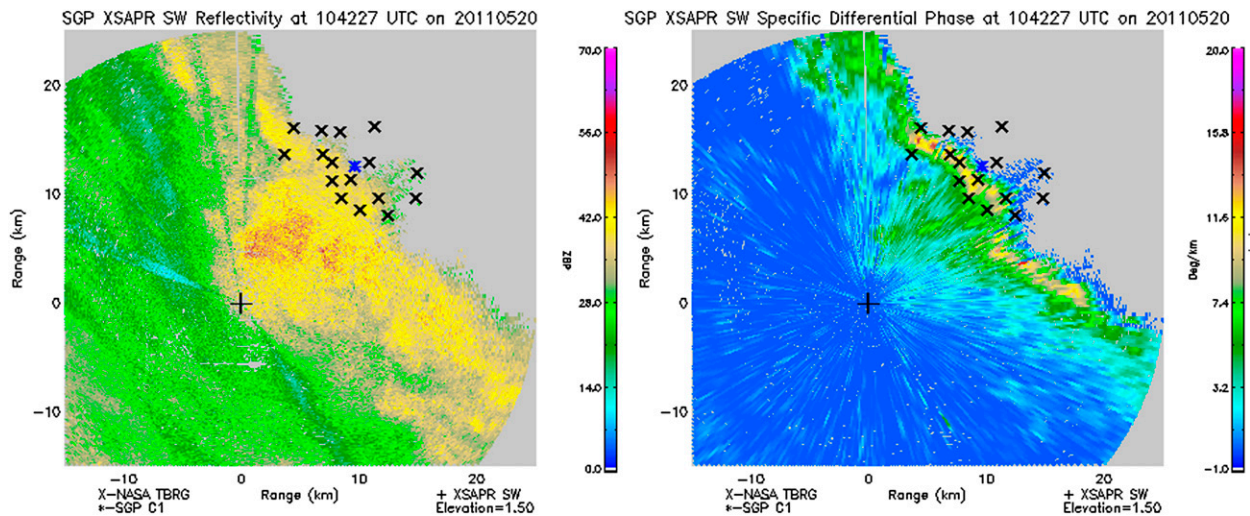


FIG. 9. Example of catastrophic measurement failure as a consequence of severe attenuation in rain over several NASA gauge locations for the 20 May 2011 squall-line event.

a unique suite of GPM ground and nearby KVN<sub>X</sub> radar observation references. The findings of this study should be applicable to other regions where deep-convective rain occurs. The key findings of this study are as follows:

- 1) Solid rainfall performance was obtained from the CSAPR-based rainfall retrievals as compared with gauges and the nearby operational KVN<sub>X</sub> reference. These products were shown to have an absolute bias of less than 0.5 mm and an RMSE of less than 4 mm for accumulations under 20 mm.
- 2) During the MC3E campaign period for methods tested, an optimal rainfall performance was observed when using the CSAPR system and capitalizing on rainfall relations designed around specific-attenuation estimates. CSAPR rainfall relationships using specific differential phase were also found to be preferable to the reference KVN<sub>X</sub>. These relations were the optimal campaign choice within heavier-rain conditions having gauge accumulations greater than 10 mm, provided these measurements were available (no beam extinction).
- 3) XSAPR methods were shown to perform comparably to KVN<sub>X</sub> and CSAPR methods for the Oklahoma events having lower gauge accumulations of less than 5–10 mm. Significant attenuation in rain and frequent extinction of the radar beam limited the usefulness of XSAPR methods for higher gauge accumulations of greater than 10 mm.

*Acknowledgments.* This paper has been authored by employees of Brookhaven Science Associates, LLC, under Contract DE-AC02-98CH10886 with the U.S. Department of Energy. The publisher by accepting the

paper for publication acknowledges that the U.S. government retains a nonexclusive, paid-up, irrevocable, worldwide license to publish or reproduce the published form of this paper, or to allow others to do so, for U.S. government purposes. Author Giangrande's work is supported by the Climate Science for a Sustainable Energy Future (CSSEF) project of the Earth System Modeling (ESM) program in the DOE Office of Science. Argonne National Laboratory's work was supported by the U.S. Department of Energy Office of Science, Office of Biological and Environmental Research (OBER), under Contract DE-AC02-06CH11357. The work has been supported by the OBER of the DOE as part of the ARM Program. Adam Theisen's work was supported by Battelle–Pacific Northwest National Laboratory, Contract 206248, and his home institution CIMMS is supported by NOAA/Office of Oceanic and Atmospheric Research under U.S. Department of Commerce NOAA–University of Oklahoma Cooperative Agreement NA11OAR4320072. The authors thank Dr. Alexander Ryzhkov for support on implementation of specific-attenuation-based rainfall methods, associated comments, and considerations. We thank Michael Jensen of BNL, Virendra Ghate of ANL, and Randy Pepler of OU-CIMMS for internal reviews of this manuscript.

#### REFERENCES

- Ackerman, T. P., and G. M. Stokes, 2003: The Atmospheric Radiation Measurement Program. *Phys. Today*, **56** (1), 38–44, doi:10.1063/1.1554135.
- Anagnostou, E. N., W. F. Krajewski, and J. Smith, 1999: Uncertainty quantification of mean-areal radar-rainfall estimates. *J. Atmos. Oceanic Technol.*, **16**, 206–215, doi:10.1175/1520-0426(1999)016<0206:UQOMAR>2.0.CO;2.

- Austin, P. M., 1987: Relation between measured radar reflectivity and surface rainfall. *Mon. Wea. Rev.*, **115**, 1053–1070, doi:[10.1175/1520-0493\(1987\)115<1053:RBMRRRA>2.0.CO;2](https://doi.org/10.1175/1520-0493(1987)115<1053:RBMRRRA>2.0.CO;2).
- Borowska, L., D. Zrnić, A. Ryzhkov, P. Zhang, and C. Simmer, 2011: Polarimetric estimates of a 1-month accumulation of light rain with a 3-cm wavelength radar. *J. Hydrometeorol.*, **12**, 1024–1039, doi:[10.1175/2011JHM1339.1](https://doi.org/10.1175/2011JHM1339.1).
- Bringi, V. N., and V. Chandrasekar, 2001: *Polarimetric Doppler Weather Radar*. Cambridge University Press, 636 pp.
- , T. D. Keenan, and V. Chandrasekar, 2001: Correcting C-band radar reflectivity and differential reflectivity data for rain attenuation: A self-consistent method with constraints. *Trans. IEEE Geosci. and Remote Sens.*, **39**, 1906–1915, doi:[10.1109/36.951081](https://doi.org/10.1109/36.951081).
- Bukovsky, M. S., and D. J. Karoly, 2011: A regional modeling study of climate change impacts on warm-season precipitation in the central United States. *J. Climate*, **24**, 1985–2002, doi:[10.1175/2010JCLI3447.1](https://doi.org/10.1175/2010JCLI3447.1).
- Caine, S., T. P. Lane, P. T. May, C. Jakob, S. T. Siems, M. J. Manton, and J. Pinto, 2013: Statistical assessment of tropical convection-permitting model simulations using a cell-tracking algorithm. *Mon. Wea. Rev.*, **141**, 557–581, doi:[10.1175/MWR-D-11-00274.1](https://doi.org/10.1175/MWR-D-11-00274.1).
- Chandrasekar, V., E. Gorgucci, and G. Scarchilli, 1993: Optimization of multiparameter radar estimates of rainfall. *J. Appl. Meteor.*, **32**, 1288–1293, doi:[10.1175/1520-0450\(1993\)032<1288:OOMREO>2.0.CO;2](https://doi.org/10.1175/1520-0450(1993)032<1288:OOMREO>2.0.CO;2).
- Ciach, G. J., 2003: Local random errors in tipping-bucket rain gauge measurements. *J. Atmos. Oceanic Technol.*, **20**, 752–759, doi:[10.1175/1520-0426\(2003\)20<752:LREITB>2.0.CO;2](https://doi.org/10.1175/1520-0426(2003)20<752:LREITB>2.0.CO;2).
- , and W. F. Krajewski, 1999: On the estimation of radar rainfall error variance. *Adv. Water Resour.*, **22**, 585–595, doi:[10.1016/S0309-1708\(98\)00043-8](https://doi.org/10.1016/S0309-1708(98)00043-8).
- , —, and G. Villarini, 2007: Product-error-driven uncertainty model for probabilistic quantitative precipitation estimation with NEXRAD data. *J. Hydrometeorol.*, **8**, 1325–1347, doi:[10.1175/2007JHM814.1](https://doi.org/10.1175/2007JHM814.1).
- Cifelli, R., W. A. Petersen, L. D. Carey, S. A. Rutledge, and M. A. F. da Silva Dias, 2002: Radar observations of the kinematic, microphysical, and precipitation characteristics of two MCSs in TRMM LBA. *J. Geophys. Res.*, **107**, 8077, doi:[10.1029/2000JD0002642002](https://doi.org/10.1029/2000JD0002642002).
- , V. Chandrasekar, S. Lim, P. C. Kennedy, Y. Wang, and S. A. Rutledge, 2011: A new dual-polarization radar rainfall algorithm: Application in Colorado precipitation events. *J. Atmos. Oceanic Technol.*, **28**, 352–364, doi:[10.1175/2010JTECHA1488.1](https://doi.org/10.1175/2010JTECHA1488.1).
- Cunha, L. K., J. A. Smith, M. L. Baeck, and W. F. Krajewski, 2013: An early performance evaluation of the NEXRAD dual-polarization radar rainfall estimates for urban flood applications. *Wea. Forecasting*, **28**, 1478–1497, doi:[10.1175/WAF-D-13-00046.1](https://doi.org/10.1175/WAF-D-13-00046.1).
- Dai, A., 2006: Precipitation characteristics in eighteen coupled climate models. *J. Climate*, **19**, 4605–4630, doi:[10.1175/JCLI3884.1](https://doi.org/10.1175/JCLI3884.1).
- Del Genio, A. D., J. Wu, and Y. Chen, 2012: Characteristics of mesoscale organization in WRF simulations of convection during TWP-ICE. *J. Climate*, **25**, 5666–5688, doi:[10.1175/JCLI-D-11-00422.1](https://doi.org/10.1175/JCLI-D-11-00422.1).
- Dirmeyer, P. A., and Coauthors, 2012: Simulating the diurnal cycle of rainfall in global climate models: Resolution versus parameterization. *Climate Dyn.*, **39**, 399–418, doi:[10.1007/s00382-011-1127-9](https://doi.org/10.1007/s00382-011-1127-9).
- Doviak, R. J., and D. S. Zrnić, 1993: *Doppler Radar and Weather Observations*. Academic Press, 458 pp.
- Duchon, C., and G. R. Essenberg, 2001: Comparative rainfall observations from pit and aboveground rain gauges with and without wind shields. *Water Resour. Res.*, **37**, 3253–3263, doi:[10.1029/2001WR000541](https://doi.org/10.1029/2001WR000541).
- , C. Fiebrich, and D. Grimsley, 2014: Using high-speed photography to study undercatch in tipping-bucket rain gauges. *J. Atmos. Oceanic Technol.*, **31**, 1330–1336, doi:[10.1175/JTECH-D-13-00169.1](https://doi.org/10.1175/JTECH-D-13-00169.1).
- Fiebrich, C. A., D. L. Grimsley, R. A. McPherson, K. A. Kesler, and G. R. Essenberg, 2006: The value of routine site visits in managing and maintaining quality data from the Oklahoma Mesonet. *J. Atmos. Oceanic Technol.*, **23**, 406–416, doi:[10.1175/JTECH1852.1](https://doi.org/10.1175/JTECH1852.1).
- Fulton, R. A., J. P. Breidenbach, D.-J. Seo, D. A. Miller, and T. O'Bannon, 1998: The WSR-88D rainfall algorithm. *Wea. Forecasting*, **13**, 377–395, doi:[10.1175/1520-0434\(1998\)013<0377:TWRA>2.0.CO;2](https://doi.org/10.1175/1520-0434(1998)013<0377:TWRA>2.0.CO;2).
- Giangrande, S. E., and A. V. Ryzhkov, 2005: Calibration of dual-polarization radar in the presence of partial beam blockage. *J. Atmos. Oceanic Technol.*, **22**, 1156–1166, doi:[10.1175/JTECH1766.1](https://doi.org/10.1175/JTECH1766.1).
- , and —, 2008: Estimation of rainfall based on the results of polarimetric echo classification. *J. Appl. Meteor. Climatol.*, **47**, 2445–2462, doi:[10.1175/2008JAMC1753.1](https://doi.org/10.1175/2008JAMC1753.1).
- , S. Collis, J. Straka, A. Protat, C. Williams, and S. Krueger, 2013a: A summary of convective-core vertical velocity properties using ARM UHF wind profilers in Oklahoma. *J. Appl. Meteor. Climatol.*, **52**, 2278–2295, doi:[10.1175/JAMC-D-12-0185.1](https://doi.org/10.1175/JAMC-D-12-0185.1).
- , R. McGraw, and L. Lei, 2013b: An application of linear programming to polarimetric radar differential phase processing. *J. Atmos. Oceanic Technol.*, **30**, 1716–1729, doi:[10.1175/JTECH-D-12-00147.1](https://doi.org/10.1175/JTECH-D-12-00147.1).
- Gourley, J. J., P. Tabary, and J. Parent du Chatelet, 2007: Empirical estimation of attenuation from differential propagation phase measurements at C band. *J. Appl. Meteor. Climatol.*, **46**, 306–317, doi:[10.1175/JAM2464.1](https://doi.org/10.1175/JAM2464.1).
- , S. E. Giangrande, Y. Hong, Z. Flaming, T. Schuur, and J. A. Vrugt, 2010: Impacts of polarimetric radar observations on hydrologic simulation. *J. Hydrometeorol.*, **11**, 781–796, doi:[10.1175/2010JHM1218.1](https://doi.org/10.1175/2010JHM1218.1).
- Gu, J.-Y., A. Ryzhkov, P. Zhang, P. Neilley, M. Knight, B. Wolf, and D.-I. Lee, 2011: Polarimetric attenuation correction in heavy rain at C band. *J. Appl. Meteor. Climatol.*, **50**, 39–58, doi:[10.1175/2010JAMC2258.1](https://doi.org/10.1175/2010JAMC2258.1).
- Guy, N., X. Zeng, S. A. Rutledge, and W.-K. Tao, 2013: Comparing the convective structure and microphysics in two Sahelian mesoscale convective systems: Radar observations and CRM simulations. *Mon. Wea. Rev.*, **141**, 582–601, doi:[10.1175/MWR-D-12-00053.1](https://doi.org/10.1175/MWR-D-12-00053.1).
- Hou, A. Y., and Coauthors, 2014: The Global Precipitation Measurement (GPM) Mission. *Bull. Amer. Meteor. Soc.*, **95**, 701–722, doi:[10.1175/BAMS-D-13-00164.1](https://doi.org/10.1175/BAMS-D-13-00164.1).
- Houze, R. A., M. I. Biggerstaff, S. A. Rutledge, and B. F. Smull, 1989: Interpretation of Doppler weather radar displays of midlatitude mesoscale convective systems. *Bull. Amer. Meteor. Soc.*, **70**, 608–619, doi:[10.1175/1520-0477\(1989\)070<0608:IODWRD>2.0.CO;2](https://doi.org/10.1175/1520-0477(1989)070<0608:IODWRD>2.0.CO;2).
- Hubbert, J., and V. N. Bringi, 1995: An iterative filtering technique for the analysis of copolar differential phase and dual-frequency radar measurements. *J. Atmos. Oceanic Technol.*, **12**, 643–648, doi:[10.1175/1520-0426\(1995\)012<0643:AIFTF>2.0.CO;2](https://doi.org/10.1175/1520-0426(1995)012<0643:AIFTF>2.0.CO;2).
- Iguchi, T., T. Matsui, A. Tokay, P. Kollias, and W.-K. Tao, 2012: Two distinct modes in one-day rainfall event during MC3E

- field campaign: Analyses of disdrometer observations and WRF-SBM simulation. *Geophys. Res. Lett.*, **39**, L24805, doi:10.1029/2012GL053329.
- Jensen, M. P., and Coauthors, 2010: Midlatitude Continental Convective Clouds Experiment (MC3E) science plan. U.S. Department of Energy Doc. DOE/SC-ARM/10-004, 31 pp. [Available online at <http://www.arm.gov/publications/programdocs/doe-sc-arm-10-004.pdf?id=17>.]
- Krajewski, W. F., and J. A. Smith, 2002: Radar hydrology: Rainfall estimation. *Adv. Water Resour.*, **25**, 1387–1394, doi:10.1016/S0309-1708(02)00062-3.
- Mather, J. H., and J. W. Voyles, 2013: The ARM Climate Research Facility: A review of structure and capabilities. *Bull. Amer. Meteor. Soc.*, **94**, 377–392, doi:10.1175/BAMS-D-11-00218.1.
- Matrosov, S. Y., D. E. Kingsmill, B. E. Martner, and F. M. Ralph, 2005: The utility of X-band polarimetric radar for quantitative estimates of rainfall parameters. *J. Hydrometeorol.*, **6**, 248–262, doi:10.1175/JHM424.1.
- , R. Cifelli, P. C. Kennedy, S. W. Nesbitt, S. A. Rutledge, V. N. Bringi, and B. E. Martner, 2006: A comparative study of rainfall retrievals based on specific differential phase shifts at X- and S-band radar frequencies. *J. Atmos. Oceanic Technol.*, **23**, 952–963, doi:10.1175/JTECH1887.1.
- Matsui, T., D. Mocko, M.-I. Lee, W.-K. Tao, M. J. Suarez, and R. A. Pielke Sr., 2010: Ten-year climatology of summertime diurnal rainfall rate over the conterminous U.S. *Geophys. Res. Lett.*, **37**, L13807, doi:10.1029/2010GL044139.
- Milbrandt, J. A., and M. K. Yau, 2006: A multimoment bulk microphysics parameterization. Part III: Control simulation of a hailstorm. *J. Atmos. Sci.*, **63**, 3114–3136, doi:10.1175/JAS3816.1.
- Otto, T., and H. W. J. Ruschenberg, 2011: Estimation of specific differential phase and differential backscatter phase from polarimetric weather radar measurements of rain. *IEEE Geosci. Remote Sens. Lett.*, **8**, 988–992, doi:10.1109/LGRS.2011.2145354.
- Park, S.-G., V. N. Bringi, V. Chandrasekar, M. Maki, and K. Iwanami, 2005a: Correction of radar reflectivity and differential reflectivity for rain attenuation at X band. Part I: Theoretical and empirical basis. *J. Atmos. Oceanic Technol.*, **22**, 1621–1632, doi:10.1175/JTECH1803.1.
- , M. Maki, K. Iwanami, V. N. Bringi, and V. Chandrasekar, 2005b: Correction of radar reflectivity and differential reflectivity for rain attenuation at X band. Part II: Evaluation and application. *J. Atmos. Oceanic Technol.*, **22**, 1633–1655, doi:10.1175/JTECH1804.1.
- Pepler, A. S., and P. T. May, 2012: A robust error-based rain estimation method for polarimetric radar. Part II: Case study. *J. Appl. Meteor. Climatol.*, **51**, 1702–1713, doi:10.1175/JAMC-D-11-0159.1.
- Rodríguez-Iturbe, I., and J. M. Mejía, 1974: The design of rainfall networks in time and space. *Water Resour. Res.*, **10**, 713–728, doi:10.1029/WR010i004p00713.
- Ryzhkov, A. V., 2007: The impact of beam broadening on the quality of radar polarimetric data. *J. Atmos. Oceanic Technol.*, **24**, 729–744, doi:10.1175/JTECH2003.1.
- , and D. Zrnic, 1998: Beamwidth effects on the differential phase measurements of rain. *J. Atmos. Oceanic Technol.*, **15**, 624–634, doi:10.1175/1520-0426(1998)015<0624:BEOTDP>2.0.CO;2.
- , S. E. Giangrande, V. M. Melnikov, and T. J. Schuur, 2005a: Calibration issues of dual-polarization radar measurements. *J. Atmos. Oceanic Technol.*, **22**, 1138–1155, doi:10.1175/JTECH1772.1.
- , —, and T. J. Schuur, 2005b: Rainfall estimation with a polarimetric prototype of WSR-88D. *J. Appl. Meteor.*, **44**, 502–515, doi:10.1175/JAM2213.1.
- , T. J. Schuur, D. W. Burgess, P. L. Heinselman, S. E. Giangrande, and D. S. Zrnic, 2005c: The Joint Polarization Experiment: Polarimetric rainfall measurements and hydrometeor classification. *Bull. Amer. Meteor. Soc.*, **86**, 809–824, doi:10.1175/BAMS-86-6-809.
- , M. Diederich, P. Zhang, and C. Simmer, 2014: Potential utilization of specific attenuation for rainfall estimation, mitigation of partial beam blockage, and radar networking. *J. Atmos. Oceanic Technol.*, **31**, 599–619, doi:10.1175/JTECH-D-13-00038.1.
- Schumacher, C., R. A. Houze, and I. Kraucunas, 2004: The tropical dynamical response to latent heating estimates derived from the TRMM precipitation radar. *J. Atmos. Sci.*, **61**, 1341–1358, doi:10.1175/1520-0469(2004)061<1341:TTDRTL>2.0.CO;2.
- Seo, B.-C., and W. F. Krajewski, 2010: Scale dependence of radar rainfall uncertainty: Initial evaluation of NEXRAD's new super-resolution data for hydrologic applications. *J. Hydrometeorol.*, **11**, 1191–1198, doi:10.1175/2010JHM1265.1.
- Shafer, M. A., C. A. Fiebrich, D. Arndt, S. E. Fredrickson, and T. W. Hughes, 2000: Quality assurance procedures in the Oklahoma Mesonet. *J. Atmos. Oceanic Technol.*, **17**, 474–494, doi:10.1175/1520-0426(2000)017<0474:QAPITO>2.0.CO;2.
- Sieck, L. C., S. J. Burges, and M. Steiner, 2007: Challenges in obtaining reliable measurements of point rainfall. *Water Resour. Res.*, **43**, W01420, doi:10.1029/2005WR004519.
- Solomon, S., D. Qin, M. Manning, Z. Chen, M. Marquis, K. Averyt, M. Tignor, and H. L. Miller Jr., Eds., 2007: *Climate Change 2007: The Physical Science Basis*. Cambridge University Press, 996 pp.
- Tabary, P., A. Boumahmoud, H. Andrieu, R. Thompson, A. Illingworth, E. LeBouar, and J. Testud, 2011: Evaluation of two “integrated” polarimetric quantitative precipitation estimation (QPE) algorithms at C band. *J. Hydrol.*, **405**, 248–260, doi:10.1016/j.jhydrol.2011.05.021.
- Testud, J., E. Le Bouar, E. Obligis, and M. Ali-Mehenni, 2000: The rain profiling algorithm applied to polarimetric weather radar. *J. Atmos. Oceanic Technol.*, **17**, 332–356, doi:10.1175/1520-0426(2000)017<0332:TRPAAT>2.0.CO;2.
- Thurai, M., V. N. Bringi, L. D. Carey, P. Gatlin, E. Schultz, and W. A. Petersen, 2012: Estimating the accuracy of polarimetric radar-based retrievals of drop-size distribution parameters and rain rate: An application of error variance separation using radar-derived spatial correlations. *J. Hydrometeorol.*, **13**, 1066–1079, doi:10.1175/JHM-D-11-070.1.
- Tokay, A., P. G. Bashor, and V. L. McDowell, 2010: Comparison of rain gauge measurements in the mid-Atlantic region. *J. Hydrometeorol.*, **11**, 553–565, doi:10.1175/2009JHM1137.1.
- Varble, A., and Coauthors, 2011: Evaluation of cloud-resolving model intercomparison simulations using TWP-ICE observations: Precipitation and cloud structure. *J. Geophys. Res.*, **116**, D12206, doi:10.1029/2010JD015180.
- Villarini, G., P. V. Mandapaka, W. F. Krajewski, and R. J. Moore, 2008: Rainfall and sampling errors: A rain gauge perspective. *J. Geophys. Res.*, **113**, D11102, doi:10.1029/2007JD009214.
- Vulpiani, G., S. Giangrande, and F. S. Marzano, 2009: Rainfall estimation from polarimetric S-band radar measurements: Validation of a neural network approach. *J. Appl. Meteor. Climatol.*, **48**, 2022–2036, doi:10.1175/2009JAMC2172.1.
- , M. Montopoli, L. D. Passeri, A. G. Gioia, P. Giordano, and F. S. Marzano, 2012: On the use of dual-polarized C-band radar for operational rainfall retrieval in mountainous

- areas. *J. Appl. Meteor. Climatol.*, **51**, 405–425, doi:[10.1175/JAMC-D-10-05024.1](https://doi.org/10.1175/JAMC-D-10-05024.1).
- Wang, Y., and V. Chandrasekar, 2009: Algorithm for estimation of the specific differential phase. *J. Atmos. Oceanic Technol.*, **26**, 2565–2578, doi:[10.1175/2009JTECHA1358.1](https://doi.org/10.1175/2009JTECHA1358.1).
- , and —, 2010: Quantitative precipitation estimation in the CASA X-band dual-polarization radar network. *J. Atmos. Oceanic Technol.*, **27**, 1665–1676, doi:[10.1175/2010JTECHA1419.1](https://doi.org/10.1175/2010JTECHA1419.1).
- Wapler, K., T. P. Lane, P. T. May, C. Jakob, M. J. Manton, and S. T. Siems, 2010: Cloud-system-resolving model simulations of tropical cloud systems observed during the Tropical Warm Pool-International Cloud Experiment. *Mon. Wea. Rev.*, **138**, 55–73, doi:[10.1175/2009MWR2993.1](https://doi.org/10.1175/2009MWR2993.1).
- Whiton, R. C., P. L. Smith, S. G. Bigler, K. E. Wilk, and A. C. Harbuck, 1998: History of operational use of weather radar by U.S. weather services. Part II: Development of operational Doppler weather radars. *Wea. Forecasting*, **13**, 244–252, doi:[10.1175/1520-0434\(1998\)013<0244:HOOUOW>2.0.CO;2](https://doi.org/10.1175/1520-0434(1998)013<0244:HOOUOW>2.0.CO;2).
- Williams, C. R., 2012: Vertical air motion retrieved from dual-frequency profiler observations. *J. Atmos. Oceanic Technol.*, **29**, 1471–1480, doi:[10.1175/JTECH-D-11-00176.1](https://doi.org/10.1175/JTECH-D-11-00176.1).
- Wilson, J. W., and E. A. Brandes, 1979: Radar measurement of rainfall—A summary. *Bull. Amer. Meteor. Soc.*, **60**, 1048–1058, doi:[10.1175/1520-0477\(1979\)060<1048:RMORS>2.0.CO;2](https://doi.org/10.1175/1520-0477(1979)060<1048:RMORS>2.0.CO;2).
- Xie, S. C., R. T. Cederwall, and M. Zhang, 2004: Developing long-term single-column model/cloud system-resolving model forcing data using numerical weather prediction products constrained by surface and top of the atmosphere observations. *J. Geophys. Res.*, **109**, D01104, doi:[10.1029/2003JD004045](https://doi.org/10.1029/2003JD004045).
- Zawadzki, I. I., 1973: Errors and fluctuations of raingauge estimates of areal rainfall. *J. Hydrol.*, **18**, 243–255, doi:[10.1016/0022-1694\(73\)90050-4](https://doi.org/10.1016/0022-1694(73)90050-4).